Dysfunction of voltage-gated K^+ Channels *Kv1.1* in sciatic nerve causes spontaneous and stress-induced neuromuscular hyperexcitability

Brunetti O[1], Imbrici P[1], Botti FM[1], Pettorossi VE[1], D'Adamo MC[1], Valentino M[4], Zammit C[2] Mora M[5], Di Giovanni G[3], Muscat R[3] and Pessia M[1]*

[1]*Section of Human Physiology, University of Perugia School of Medicine, Perugia, Italy*

Department of Anatomy[2], Physiology & Biochemistry[3] and Pathology[4], University of Malta

[5]*Istituto Neurologico Carlo Besta, Milan, Italy*

* Corresponding author: Mauro Pessia, Ph.D., Department of Internal Medicine, Section of Human Physiology, University of Perugia, Via del Giochetto, I-06126 Perugia, Italy.

Tel: +39.75.5857375; Fax: +39.75.5857371; e-mail: pessia@unipg.it

Number of pages: 31; number of figures: 10; number of words for abstract (256), introduction (572), materials and methods (1809), results (2021), discussion (1845), references (861) and figure legends (1718). The authors declare that there is no conflict of interest

Acknowledgements: We thank Massimo Pierucci and Samanta Keppoch for their contributions to this study. This work was supported by COMPAGNIA di San Paolo (Turin) "*Programma Neuroscienze*", Telethon and Fondazione Cassa di Risparmio di Perugia.

SUMMARY

Episodic ataxia type 1 (EA1) is an autosomal dominant neurological disorder characterized by *myokymia* and attacks of ataxic gait precipitated by stress events. Several genetic mutations have been identified in the *Shaker*-like K^+ channel *Kv1.1* (*KCNA1*) of EA1 individuals, including the V408A which results in remarkable channel dysfunction. By inserting heterozygous V408A mutation in one *Kv1.1* allele, a mouse model of EA1 has been generated ($Kv1.1^{V408A/+}$). Here, we hypothesized that dysfunction of *Kv1.1* channels in sciatic nerve of $Kv1.1^{V408A/+}$ ataxia mice leads to neuromuscular hyperexcitability and to abnormal susceptibility to different stressors. By using *in vivo* preparations of *lateral gastrocnemius* (*LG*) nerve–muscle from $Kv1.1^{+/+}$ and $Kv1.1^{V408A/+}$ mice, we show that the mutant animals exhibit spontaneous *myokymic* discharges consisting of repeated singlets, duplets or multiplets, despite sciatic nerve axotomy. Two-photon laser scanning microscopy from the sciatic nerve, *ex vivo*, revealed spontaneous Ca^{2+} signals that occurred abnormally only in preparations dissected from $Kv1.1^{V408A/+}$ mice. The spontaneous bursting activity, as well as that evoked by motor nerve stimulation, was exacerbated by muscle fatigue, ischemia and low temperatures. These stressors also increased the amplitude of muscle compound action potential. Such abnormal neuromuscular transmission did not alter fiber type composition neuromuscular junction and vascularization of *LG* muscle analyzed by light and electron microscopy. These findings indicate that dysfunction of *Kv1.1* channels results in sciatic nerve hyperexcitability and myokymia/neuromyotonia in $Kv1.1^{V408A/+}$ ataxia mice. Moreover, this study sheds new light on the functional role played by K^+ channels segregated under the myelin sheath, which becomes crucial in certain situations of physiological stress.

INTRODUCTION

Episodic ataxia type 1 (EA1) is an autosomal dominant neurological disorder affecting both the central nervous system (CNS) and peripheral nervous system (PNS) that results from heterozygous mutations in the *Shaker*-like K^+ channel Kv1.1 (*KCNA1*; *for review see* Pessia and Hanna, 2010; Kullmann, 2010; Rajakulendran et al., 2007). The hallmark of EA1 is continuous myokymia (*muscle twitching with a rippling appearance, intermittent cramps and stiffness*) and episodic attacks of generalized ataxia with jerking movements of head, arms, legs and loss of balance. How dysfunction of *Kv1.1* channels triggers these episodes is entirely unknown. Other neuromuscular findings include unusual hypercontracted posture, abdominal wall muscle contraction, elbow, hip, and knee contractions and shortened Achilles tendons that may result in tiptoe walking. Myokymia is commonly detected in individuals with EA1 during and between attacks and, usually, it is evident as a fine rippling in perioral or periorbital muscles and by lateral finger movements when the hands are held in a relaxed, prone position. Electromyographic (EMG) recordings show that spontaneous myokymia is distinguished by a pattern of either rhythmically or arrhythmically occurring singlets, duplets, or multiplets. Both attacks of ataxia and periods of more intense myokymic activity are precipitated by a number of stresses including exercise or fatigue. In some individuals myokymic discharges may become apparent or gradually rise in frequency and intensity after the application of regional ischemia. Temperature changes may affect myokymia and trigger attacks of ataxia (Eunson et al 2000). It is has been postulated that myokymia and neuromyotonia result from motor unit hyperexcitability, although, the neurophysiological mechanisms underlying these symptoms remain largely obscure.

A *knock-in* animal model of EA1 has been generated by inserting the heterozygous EA1 mutation V408A in one Kv1.1 allele: $Kv1.1^{V408A/+}$. These animals displayed abnormal cerebellar basket cell – Purkinje cell synaptic transmission. Furthermore, isoproterenol administration to $Kv1.1^{V408A/+}$ animals, a procedure that produces stress-fear responses, induced motor dysfunctions in

Kv1.1$^{V408A/+}$ animals similar to EA1 (Herson et al., 2003). This evidence clearly demonstrated that dysfunction of *Kv1.1* channels, caused by a very subtle heterozygous mutation in *Kcna1* (*valine to alanine substitution*), alters the transmission of signals within a distinct cerebellar circuitry. To date, the neuromuscular transmission of *Kv1.1*$^{V408A/+}$ animals has not been investigated.

Action potentials (AP) propagate rapidly in myelinated axons by saltatory conduction. The juxtaparanodal regions of myelinated axons express a macromolecular membrane complex composed of *Kv1.1*, *Kv1.2*, their accessory subunit *Kvβ1.2* and the contactin-associated protein Caspr2 (Vacher et al., 2008; Wang et al., 1993; Poliak et al., 1999). This macromolecular complex has been found also at the level of the axons branching in both the CNS and PNS (Tsaur et al., 1992; Wang et al., 1994). The absence of myelin-covered K^+ channels *Kv1.1*, caused by genetic inactivation of *Kcna1*, results in temperature-sensitive neuromuscular transmission (Zhou et al., 1998, 1999, 2001). Here, we postulated that dysfunction of *Kv1.1* channels in *Kv1.1*$^{V408A/+}$ ataxia mice leads to sciatic nerve hyperexcitability and to abnormal susceptibility of the neuromuscular transmission to physiologically relevant stressors. Indeed, by using both *in vivo* and *ex vivo LG* muscle-nerve preparations from *Kv1.1*$^{+/+}$ and *Kv1.1*$^{V408A/+}$ mice we show that such mutation results in spontaneous muscle discharges and abnormal Ca^{2+} signaling in sciatic nerve. Moreover, stresses such as fatigue, ischemia and lower temperatures induce delayed repetitive discharges in mutant mice only. Overall, this study sheds new light on the functional role played by juxtaparanodal K^+ channels composed of *Kv1.1* subunits which becomes crucial under certain situations of physiological stress.

METHODS

Surgical procedures

This study was carried out on laboratory bred adult (P90±10 days) *Kcna1*$^{+/+}$ and *Kcna1*$^{V408A/+}$ male mice. The procedures that involve the use of animals are in accordance with the regulations of the Italian Animal Welfare Act and approved by the local Authority Veterinary Service and in accordance with the NIH Guide for the Care and Use of Laboratory Animals. Sodium penthotal at the indicated dosage (50 mg Kg^{-1} i.p.) was used to induce and maintain anesthesia. The level of anesthesia was verified by a stable heart rate and pupillary diameter throughout the experiment. The trachea was cannulated and end-tidal CO_2 concentration was monitored throughout all experiments. When necessary, the animals were artificially ventilated. The femoral blood pressure was measured and maintained at a constant level within the physiological range. The body temperature was controlled by maintaining the rectal temperature close to 37.5 °C using a feedback-regulated heating blanket. Under a dissecting microscope, the nerve and the *LG* muscle were isolated in the poplitea fossa and all other hindlimb muscles were denervated. The central stump of the sciatic nerve was sectioned at its entry into the posterior leg fossa. The legs were fixed by clamping the hip, knee and ankle. The Achilles' tendon was detached from its distal insertion and connected to a strain gauge. A recording chamber bordering the surgery site was applied in order to submerge the *LG* muscle and its nerve in mineral oil that was maintained at 37 °C by using a servocontrolled thermoresistance. A pair of platinum stimulating wires were placed on the sciatic nerve, with the cathode towards the muscle. To activate motor fibres, single pulses of 0.1 ms duration and with 0.18—0.22 μA intensity were delivered. The intensity of the stimulus was adjusted in order to evoke half-maximal mCAP.

EMG recording

For bipolar recordings of spontaneous or evoked EMG activity, paired hook wires (0.1 mm diameter, copper) were inserted by hollow needles into the medial portion of the *LG* muscle, approximately 1 mm above nerve entry. The electric signal was amplified by using a Grass P511 amplifier (Quincy, MA, USA) with the filters set at 10-500 Hz and stored using an ATMIO 16E10 acquisition and analysis system (National Instrument, Austin, TX, USA). The EMG activity was rectified and integrated. To exclude the noise from the signal, any electrical activity of amplitude lower than any recognizable motor unit EMG activity was eliminated.

Muscular tension

LG muscle tension was measured by using a force transducer (F03 Grass, Quincy, MA, USA). The optimal muscle length (L_0) for the maximal twitch force was determined and all force recordings were then performed at this optimal length. Most of the muscle mechanical recordings were performed in isometric condition with the external load exceeding the maximal force production (4 g load). Some experiments were performed in quasi-isotonic condition with a minimal load (10 mg load). Contractions were elicited by electrical stimulation delivered by bipolar platinum electrodes placed on the isolated nerve of the *LG* muscle.

Muscle fatigue

LG muscle fatigue was induced by high frequency stimulation (HFS) trains delivered to the *LG* motor nerve (a train lasted 600 ms at a fusion frequency of 85 Hz, with a 1 s interval between each train). To induce different degrees of fatigue, HFS trains lasting 30, 60, 180 s were applied. The effect of fatigue on the muscle force was evaluated by measuring both the force decay during HFS trains and the twitch peak tension elicited 10 s before and after stimulation. Fatigue index was calculated as the area on the envelope around the force curve for the second minute divided by that for the first minute of the test.

Muscular ischemia and temperature

To provoke muscle ischemia, the artery and venous vessels supplying the *LG* muscle were temporarily occluded for 3 minutes at their entry into the muscle using a micro-bulldog clip. The effect of ischemia on twitch force was recorded in combination with the EMG activity. The recording temperature was lowered in two degree steps from 36°C to 22°C and raised again to 36°C by changing the setting point of the thermoresistence.

Analysis of EMG recordings

The EMG activity was integrated in 1 sec epoch. The values were normalized with respect to the integrated value of the muscle compound action potential (mCAP) evoked at the beginning of each experiment (EMG integration/mCAP integration) to compare the responses obtained from different experiments. This procedure is based on the assumption that the mCAP are not different between *Kcna1*$^{+/+}$ and *Kcna1*$^{V408A/+}$ mice. To examine the time course of the responses elicited by the electrical stimulation during the early periods, EMG integration was performed in 100 msec epoch. These values were multiplied by a factor of 100 in order to obtain data comparable with those calculated in 1 second epoch. The statistical analysis was performed by using Student's paired t-test and ANOVA. A difference of $p<0.05$ was considered to be statistically significant.

LG nerve-muscle dissection and dye loading

Mice from both groups were anaesthetized with an intraperitoneal injection of chloral hydrate (4% in saline solution) and an incision was made under a surgical microscope on the left side at mid thigh level to expose the sciatic nerve via blunt dissection. The sciatic nerve in the thigh was removed along with the underlying part of the caudofemoralis muscle (still attached to the nerve by the posterior mesoneurium) and immediately transferred in a holding chamber containing aCSF gassed with 95% O_2 and 5% CO_2 at room temperature. The aCSF was composed of (mM) 126 NaCl, 3.5 KCl, 1.3 $MgCl_2$, 2 $CaCl_2$, 1.2 NaH_2PO_4, 25 $NaHCO_3$, and 10 glucose, pH 7.4.

To image Ca^{2+} signals in the sciatic nerve the whole preparation was incubated for 2 h in Fluo3-AM (Invitrogen) according with a previously published procedure (MacLean and Yuste 2005). Briefly, Fluo-3 AM (50µg) was dissolved in 48µl of DMSO and 2 µl of 20% pluronic acid to make a 1mM solution. This stock solution was then added to 5ml of oxygenated aCSF to give a final concentration in the bath of 10µM fluo-3 AM. To the same mixture, the red emitting Ca^{2+} insensitive reference indicator sulforhodamine 101 (SR-101) was added to a final concentration of 100µM (Ren *et al.,* 2000). The Ca^{2+} indicator was chosen for several reasons. Most importantly, the quantum efficiency of fluo-3 AM is relatively high and the signal-noise ratio can be greater than many of the other commercially available dyes. The SR-101 was used to image axon profiles in the nerve and to confirm through a series of image pairs collected simultaneously from both detector channels (red and green) that the regions of interest (defined by the appearance of Ca^{2+} signals) were localized within the axonal profiles.

Two-photon laser scanning microscopy

The whole *LG* nerve-muscle preparation was then transferred to a mini submerged chamber (0.5ml) with a coverglass bottom (Warner Instrument Corporation, Hamden, CT) mounted on the stage of an upright multiphoton microscope. To prevent movement during image acquisition, the preparation was secured by means of a nylon mesh glued to a U shaped platinum wire that totally submerged the tissue in a continuously flowing aCSF at a rate of 3 ml/min (oxygenated with 95% O_2/5% CO_2; warmed to 33±1°C) and washed for 1h before recording. High-resolution *ex vivo* two-photon imaging was performed with a custom-modified Olympus BX50W1 upright microscope (Olympus, Tokyo, Japan) designed for low dispersion. The system includes Keplerian beam expanders with IR introduction light paths to achieve perfect excitation efficiency and highly resolved multiphoton images. A mode-locked MaiTai HP DeepSee laser system (Spectra-Physics) with a tuneable Ti: sapphire oscillator (690-1040 nm) used as the excitation light source (pulse width < 100fs; pulse repetition rate 80Mhz) and controlled through an acousto-optical-modulator to

allow for precise changes in laser intensity. The Group Velocity Dispersion was electronically compensated by a prism-coupled pre-chirper and the beam diameter adjusted by a Keplar telescope. Images where acquired with a water-based 25X Olympus XLPLN25xWMP multiphoton objective (NA 1.05, WD 2.0) and FluoView imaging software using time-series. Excitation wavelength was 810nm. Two-channel detection of emission wavelength was achieved by using a 565-nm dichroic (Chroma) and two external photomultiplier tubes. A 515/560 bandpass filter (Chroma) was used to detect fluo-3 AM emission wavelength, and a 590/650 bandpass filter (Chroma) was used to detect SR-101 signals. Time series of fluorescent images were collected with the following parameters: 128 x 128 pixel images, optical zoom 4 x with x25 objective (N.A. 1.05), 200 frames, 850 ms/frame, 3-µs pixel dwell time, laser power of about 50 mW at sample. Bidirectional scanning was used to increase scan speed and scanners were always calibrated for XY alignment before each acquisition. Ca^{2+} signals were recorded as changes in mean pixel intensity in defined regions of interest (axonal fibres) over time and expressed as the change in fluorescence divided by the baseline fluorescence ($\Delta F/F_0$) (Ren et al 2000; MacLean and Yuste 2005). To compare the changes in fluorescence intensity recorded from the sciatic nerve of both $Kv1.1^{+/+}$ and $Kv1.1^{V408A/+}$ mice, a moving average smoothing was performed, *i.e.* an average of every five consecutive data points was calculated and plotted on a graph. Three standard deviations were then added to the moving average. Any data points of ΔF that lay outside these three standard deviations were regarded as a significant change from the mean. χ^2 analysis was then performed to assess for any statistical significant difference between the number of data points outside three standard deviations for both groups of animals.

Optical and electron microscopy

LG muscles were snap-frozen in isopentane/liquid nitrogen, and maintained in liquid nitrogen until use. Routine haematoxylin and eosin, Gomori-modified Trichrome and NADH staining were performed by using 8 µm-thick cryosections. A small fragment of muscle tissue from contralateral

LG was fixed in 4% glutaraldehyde in phosphate buffer, post-fixed in 2% osmium tetroxide, dehydrated and embedded in Spurr resin. Ultrathin sections were stained with uranyl acetate and lead citrate and examined with a Philips 410 electron microscope.

Capillary density and diameters were measured on *griffonia simplicifolia* lectin I (GSL I)-stained sections at 40X magnification using the NIH Image software version 1.62 (http://rsb.info.nih.gov/nih-image) as previously described (Zanotti et al., 2005). Twenty fields from each animal were analyzed. Briefly, fields of equal size were photographed and digitalized. By using a software, a threshold was applied to the micrographs to obtain black and white images with areas positive for lectin I in black and negative areas in white. The number of capillaries was counted and the diameters measured in each field. The mean±SD was then obtained for each group from the total of all analyzed fields. Cryosections were incubated for 120 min at room temperature in biotinylated GSL I diluted 1:200 (Vector Laboratories, Burlingame, CA, USA) and followed by a 60 min incubation in Rhodamine Red^{TM}-X-conjugated avidin diluted 1:250 (Molecular Probes, Eugene, OR, USA). Sections were examined under a Zeiss Axioplan fluorescence microscope.

RESULTS

Spontaneous neuromuscular activity in Kv1.1$^{V408A/+}$ ataxia mice

EMG recordings were carried out, *in vivo*, from *LG* muscle of *Kv1.1*$^{+/+}$ (n =10) or *Kv1.1*$^{V408A/+}$ (n = 10) mice in isometric condition at L_0. The motor nerve supplying *LG* muscle was centrally severed to eliminate the influence of the CNS on EMG activity. Spontaneous EMG activity was observed in 6 out of 15 *Kv1.1*$^{V408A/+}$ mice, while it was never observed in *Kv1.1*$^{+/+}$ mice (Fig. ***1A***). The bursting activity observed in the *Kv1.1*$^{V408A/+}$ mice consisted of patterns of singlets, duplets or multiplets of variable amplitudes (50-500 μV). The burst frequency varied among the *Kv1.1*$^{V408A/+}$ animals and ranged from 1 to 5 bursts/s. In *Kv1.1*$^{V408A/+}$ mice, displaying spontaneous EMG activity, the integrated EMG value (1 sec epoch) was similar to that of the muscle compound action potential (mCAP), evoked by electrical stimulation, so the EMG/mCAP ratio was ~1 (Fig. ***1C***). This normalized value was significantly different from that calculated for *Kv1.1*$^{+/+}$ mice ($p<0.001$). In the same group of mice, single electric pulses were delivered every one second to the peripheral stump of the *LG* motor nerve. Electric shocks evoked direct EMG responses in both groups of mice mostly characterized by typical triphasic mCAPs occurring with a distinct delay (Fig.***1B***). The electric shock also elicited early and delayed bursting activity in all *Kv1.1*$^{V408A/+}$ mice but not in *Kv1.1*$^{+/+}$ (Fig.***1B***). By normalising the integrated area of the delayed evoked activity for *Kv1.1*$^{V408A/+}$ (EMG/mCAP) we observed a significant increase of this value compared to either that evoked in *Kv1.1*$^{+/+}$ or spontaneously occurring in *Kv1.1*$^{V408A/+}$ mice (Fig.***1C***). The delayed discharges reached a maximal intensity within 300-600 msec after the electric shock and declined thereafter (Fig. ***1D***). Thus, the EMG response elicited by axon stimulation displayed a biphasic shape, denoting a sequence of events that leads to early and rebound abnormal activity.

The sciatic nerve of Kv1.1$^{V408A/+}$ mice displays spontaneous Ca^{2+} signals

To investigate the role played by the sciatic nerve in the myokymic activity observed form *Kv1.1*$^{V408A/+}$ ataxia mice, Ca^{2+} signals were recorded by fluorescent imaging of the sciatic nerve, *ex vivo,* previously loaded with the calcium sensitive dye fluo-3 AM (Lev-Ram and Ellismann 1995). In one set of experiments, the sciatic nerve branching over the *LG* muscle was visually localized. Afterward, two-photon laser scanning microscopy (2P-LSM) imaging of this structure from *Kv1.1*$^{V408A/+}$ mice revealed intense Ca^{2+} signals occurring spontaneously (Fig.***2B,E***). In another set of experiments, the localization of Ca^{2+} signals within sciatic nerve branches, dissected from *Kv1.1*$^{V408A/+}$ mice, were confirmed by using the Ca^{2+} insensitive reference indicator sulforhodamine 101 (SR-101) that allowed the direct visualization of the axon profiles in the nerve. Therefore, the fluorescence values ($\Delta F/F_0$) determined in both experimental conditions were combined. In nerves from *Kv1.1*$^{V408A/+}$ mice, Ca^{2+} signals occurred in bursts characterized by singlets, duplets or multiplets of variable amplitude and frequency that ranged from 0.8 to 4.5 bursts/s (Fig.***2B***). To estimate the overall intensity of these signals the fluorescence values ($\Delta F/F_0$) were integrated and averaged. The values for *Kv1.1*$^{V408A/+}$ nerves (n = 5) were remarkably higher then the *Kv1.1*$^{+/+}$ (n = 5; Fig.***2C***; ANOVA; $p<0.001$). Although such dramatic Ca^{2+} transients were never observed from preparations dissected from *Kv1.1*$^{+/+}$ mice and imaged as described above, some recordings displayed oscillations in fluorescence intensity (Fig. ***2A***). To provide for these changes, a moving average smoothing was calculated for each set of data of every experiment and any data points of ΔF that lay outside three standard deviations were regarded as a significant change in fluorescence from the mean (*see methods*). The χ^2 analysis revealed a remarkable statistical difference between the *Kv1.1*$^{+/+}$ and *Kv1.1*$^{V408A/+}$ data sets (Fig.***2D***; $p<0.001$). These results strongly suggest that the abnormal Ca^{2+} signals in sciatic nerve of *Kv1.1*$^{V408A/+}$ mice are due to the insertion of a heterozygous V408A mutation in their *Kcna1* gene.

Influence of muscle fatigue on LG muscle force and EMG activity

To study the responses of *LG* muscle to stress which typically mimic muscle fatigue, trains of high frequency stimulations (HFS) were applied to the *LG* motor nerve. In isometric condition at L_0, HFS trains induced similar muscle fatigue in both *Kv1.1*$^{+/+}$ (n = 15) and *Kv1.1*$^{V408A/+}$ (n= 15) mouse types. This is shown by the similar reductions of tetanic and twitch peak tension in both groups of animals (Fig.***3A,C***). The tension decreases were 62±1.5% and 63±2%, respectively ($p>0.05$; Fig.***3C***). The time constants (τ) of the tetanic tension decay and the fatigue index (FI) were also similar (*Kv1.1*$^{+/+}$: τ = 21±1 s and FI =0.53; *Kv1.1*$^{V408A/+}$: τ =25±3s and FI = 0.52; $p>0.05$; Fig.***3D,E***). Complete twitch tension recovery occurred within 25-30 min. This and its progression over time occurred similarly in both groups of mice ($p>0.05$; Fig.***3F***). HFS trains were also delivered while keeping the *Kv1.1*$^{V408A/+}$ muscle in "quasi-isotonic" condition. In this condition there was a twitch tension decrease of less than 5%, indicating that muscle fatigue was minimal (Fig.***3B***).

LG muscle tension measurements were performed concomitantly with EMG recordings (Fig.***4*** *inset*). The EMG activity in *Kv1.1*$^{+/+}$ mice remained silent before and after the tetanic stimulation throughout the entire recovery period from fatigue (Fig.***4A***). Conversely, fatigue stimulation increased spontaneous EMG bursting activity by eliciting singlets, duplets and multiplets from *Kv1.1*$^{V408A/+}$ mice (Fig.***4B***). EMG bursting was enhanced when the resting activity was present (4 out of 10 animals), while it become apparent and more intense when the spontaneous activity was absent (6 out of 10 animals). The value of the integrated spontaneous EMG activity for *Kv1.1*$^{V408A/+}$ mice became maximal ~10-15 min after the end of HFS trains, reaching ~2.5-fold increase compared to pre-fatigue values. Thereafter, it diminished to approach the pre-fatigue value (Fig.***4B,C***). Statistical comparison of the EMG integrated values calculated after the end of fatigue stimulation for *Kv1.1*$^{+/+}$ and *Kv1.1*$^{V408A/+}$ mice were significantly different ($p< 0.001$). In another group of mice the activity evoked in response to electric pulses delivered to the motor nerve was examined. The EMG activity following electric shocks remained silent in all *Kv1.1*$^{+/+}$ animals (n =

15) before and after muscle fatigue induction (Fig.***4A***). By contrast, a delayed bursting activity was recorded from *Kv1.1*$^{V408A/+}$ mice (n =15) both in silent pre-fatigue muscles (9 out of 15) and in bursting muscles (6 out of 15). The post-stimulus activity was maximal ~10 min after HFS, when it reached ~12-fold increase compared to pre-fatigue level and, then, declined to approach the control value 25-30 min later (Fig.***4B,D***). The after-discharges increased immediately after the electric shock, presented a second peak at ~300-400 msec post-stimulus and declined thereafter (Fig.***4E***). The analysis of the muscle compound action potential (mCAP) was also performed by integrating the evoked three-phasic waves before and after HSF trains. In *Kv1.1*$^{+/+}$ mice, the evoked responses showed ~15% reduction immediately after the fatiguing stimulation and returned to control level (Fig.***5A,C***). Conversely, mCAPs increased remarkably in *Kv1.1*$^{V408A/+}$ muscles, reaching a maximal amplitude (~5-fold increase) ~15 min after HSF trains (Fig.***5B,C***).

To assess the role of the degree of muscle fatigue on the induction of bursting, HFS trains were delivered while keeping the *Kv1.1*$^{V408A/+}$ muscle in "quasi-isotonic" condition. Under this condition muscle fatigue was minimal (*see* Fig.***3B***) and EMG bursting activity was neither significantly increased when spontaneously present nor elicited in silent *Kv1.1*$^{V408A/+}$ muscles (Fig.***6A***; $p>0.05$). Also the duration of HFS trains were changed in isometric conditions to induce different degrees of muscle fatigue in *Kv1.1*$^{V408A/+}$ mice. HFS trains lasting 30, 60 and 180 sec induced muscle tension decrease of ~35%, ~55% and ~62%, respectively. In all these different fatigue conditions the bursting activity, as well as the mCAP were enhanced (Fig.***6A,B***). In particular, mCAP amplitude (measured just after HFS delivery) increased linearly with tension decrease while it did not change in "quasi-isotonic" condition ($R =0.98$, $p<0.001$; Fig.***6B***).

Optical and electron microscopy analysis of LG muscle and nerve preparations

The repetitive firing of the *Kv1.1*$^{V408A/+}$ muscle fibers combined with clinical findings reporting enlargement of gastrocnemius fiber type I and II diameters in some EA1 individuals (Van Dyke *et al.,* 1975) prompted us to perform morphological studies on *LG* muscle sections and nerves derived

from *Kv1.1*$^{+/+}$ and *Kv1.1*$^{V408A/+}$ adult mice (Fig.***7A***). *LG* muscles dissected from these animals had similar muscle mass. This is demonstrated by the insignificant statistical difference between the ratios of the muscle-to-body weight, which were 5.4±0.03mg/g and 5.3±0.04mg/g, respectively (n=30; p>0.05). Histograms of the frequency distribution for fiber type I and type II diameters were constructed for both *Kv1.1*$^{+/+}$ and *Kv1.1*$^{V408A/+}$ *LG* muscles and the average diameters for both fiber types were similar (Fig.***7B-G***). Finally, the electron microcopy analysis of the neuromuscular junction also revealed not obvious differences (Fig.***7A***). We also investigated the possible effects of repetitive firing on muscle vascularization. However, neither the capillary density nor the capillary diameter of *LG* muscles for both *Kv1.1*$^{+/+}$ and *Kv1.1*$^{V408A/+}$ mice were significantly different (Fig.***8A-C***). Taken together these findings imply that the spontaneous and fatigue-induced *LG* neuromuscular hyper-excitability do not results in major morphological changes in *LG* muscles from *Kv1.1*$^{V408A/+}$ mice.

Ischemia exacerbates LG nerve-muscle excitability in Kv1.1$^{V408A/+}$ ***mice***

To induce ischemia, the artery and venous vessels supplying the *LG* nerve and muscle of *Kv1.1*$^{+/+}$ (n=5) and *Kv1.1*$^{V408A/+}$ (n=5) mice were temporarily occluded (3 min; Fig.***9*** *inset*). The effectiveness of ischemia was evaluated indirectly by measuring muscle twitch tension in isometric conditions (Fig.**9*A***). Twitch tension decreased ~60% at the end of the ischemic period, without significant differences between *Kv1.1*$^{+/+}$ and *Kv1.1*$^{V408A/+}$ muscles (p>0.05; Fig.***9A***). After vessel re-opening, twitch tension gradually recovered within ~30 min in both groups of animals. EMG activity was recorded before, during ischemia and reperfusion while delivering single electric shock to sciatic nerve. In none of these conditions after-discharges were ever detected in *Kv1.1*$^{+/+}$ mice (Fig.***9B***). Whereas, in 4 out 5 *Kv1.1*$^{V408A/+}$ animals ischemia elicited delayed activity consisting of singlets, duplets and multiplets (Fig.***9C***). In the remaining mouse, the spontaneous activity was present in resting conditions and it was increased by ischemia. The dynamics of the EMG activity enhancement and of the twitch tension decrease differed. Indeed, the former continued to increase

during the early period of reperfusion reaching a peak of activity ~5 min after vessel re-opening (Fig.***9D***). Thereafter, EMG activity decreased over a period of 20-30 min (Fig.***9D***). The electric shock induced a biphasic increase of the after-discharges which reached an early peak soon after the stimulus and a second peak at 400 msec. This activity declined within 1 sec (Fig.***9F***). Moreover, the mCAP elicited in *Kv1.1*$^{V408A/+}$ mice increased progressively, starting 2 min after ischemia induction, reached ~6-fold increase ~5 min after vessel reopening and declined thereafter (Fig.***9E***). Conversely, ischemia reduced the mCAP in *Kv1.1*$^{+/+}$ mice (Fig.***9E***). Interestingly, both the bursting activity (Fig.***9D***) and the mCAP enhancement induced by ischemia (Fig.***9E***) displayed a similar time course. The overall statistical evaluation of the effects of ischemia on the integrated values of bursting activity and mCAP calculated for *Kv1.1*$^{+/+}$ and *Kv1.1*$^{V408A/+}$ mice resulted in significant differences ($p<0.01$).

V408A mutation in Kv1.1 channels confers marked temperature-sensitivity to neuromuscular transmission in adult mice

EMG recordings were performed from *Kv1.1*$^{+/+}$ (n=7) and in *Kv1.1*$^{V408A/+}$ (n=7) mice while the temperature was lowered in two degree steps from 36°C to 22°C and raised again to 36°C by changing the setting point of the thermoresistence (Fig.***10*** *inset*). Single electrical motor nerve stimulation never elicited abnormal delayed discharges from *Kv1.1*$^{+/+}$ mice when the recording temperature was lowered (Fig.***10A***). By contrast, cooling induced post-stimulus discharges were either brought about in 5 out of 7 *Kv1.1*$^{V408A/+}$ mice or increased in the remaining 2 animals, in which discharges were present, spontaneously (Fig.***10B***). The EMG recordings were characterized by the presence of randomly distributed singlets, duplets and multiplets that resembled those observed under fatigue and ischemia. The analysis of the integrated EMG activity (calculated during the post-stimulus periods and every two degrees of cooling) showed that bursting was either evoked or enhanced when temperature was lowered below 28-26°C (Fig.***10C***). It reached a maximal intensity at 22°C, whereby ~12-fold increase compared to the control value was

calculated. Bursting was more intense immediately after the electric shock and declined thereafter (Fig.***10D***). The analysis of mCAP at 22°C yielded a slight decrease for *Kv1.1*$^{+/+}$ and a slight increase for *Kv1.1*$^{V408A/+}$muscles, which resulted in a significant difference between the two groups of animals (Fig.***10E***).

DISCUSSION

The main finding of this study is that *Kv1.1*$^{V408A/+}$ ataxia mice display hyper-excitability of the motor units which is exacerbated by stress events such as fatigue, ischemia and lower temperatures. The hyper-excitability is demonstrated by the abnormal presence of EMG bursting activity and Ca^{2+} signals in resting conditions and by the stress-induced enhancement of both bursting and mCAP. This bursting and such large Ca^{2+} signals have never been observed in *Kv1.1*$^{+/+}$ mice. These findings are pertinent to the understanding of the mechanisms underlying EA1 symptoms caused by the altered transmission of impulses in myelinated PNS nerves such as neuromyotonia/myokymia, difficulty in breathing (Shook et al 2008) and their abnormal susceptibility to stressors. Furthermore, this study highlights the crucial role played by *Kv1.1* channels in the PNS also during physiologically relevant stress events.

Hyper-excitability of the sciatic nerve

The peripheral source of spontaneous and evoked bursts from *Kv1.1*$^{V408A/+}$ mice is confirmed in our *in vivo* experimental setting since they are observed in the presence of centrally severed sciatic nerve. The hyper-excitability of the sciatic nerve of *Kv1.1*$^{V408A/+}$ mice is also demonstrated by the presence of abnormal Ca^{2+} signals in branches of the nerve, *ex vivo*. Noteworthy, the pattern of both EMG activity and of the Ca^{2+} signals recorded from *Kv1.1*$^{V408A/+}$ preparations is remarkably similar, denoting close correlations between these events. It has been shown that the sources of the

Ca^{2+} signals associated with sciatic nerve activity are Ca^{2+} entry through plasma membrane channels as well as the release of Ca^{2+} from intracellular stores in both axons and Schwann cells (Lev-Ram and Ellismann 1995; Zhang et al., 2006, 2010; Chiu et al., 1999, 2011). Based on this and our evidence, we suspect that the spontaneous electrical discharges occurring in the axon of sciatic nerve from *Kv1.1*$^{V408A/+}$ animals activates Ca^{2+} influx and Na^{+} dependent release of Ca^{2+} from mitochondria at nodes of Ranvier. Furthermore, such discharges are expected to depolarize the nearby Schwann cells, inducing Ca^{2+} entry through plasma membrane channels as well as Ca^{2+} activated Ca^{2+} release from ryanodine-dependent stores. Taken together these findings reveal that a point mutation that causes well documented *Kv1.1* and *Kv1.1*/*Kv1.2* channel dysfunction (Adelman et al., 1995; D'Adamo et al., 1998, 1999; Zerr et al., 1998), triggers spontaneous electrical discharges in peripheral motor units and increases their responsiveness to electrical stimuli. The presence of *Kv1.1* channels at both juxtaparanodal regions and branch points of sciatic nerves and their absence at both the end-plate and muscle fibers (Arroyo et al., 1999; Vacher et al., 2008; Zhou et al., 1998) suggest that the place of induction of hyper-excitability is the axon and its terminals. Experiments performed by using *Kv1.1* knock-out mice indicate that the sources of abnormal activity are the terminals of the motor nerve. It has been proposed that the progressive reduction of inter-nodal length and the lack of juxtaparanodal *Kv1.1* channels lead to re-entrant excitation of nodes (Zhou et al., 1998, 1999). Our evidence obtained by using *Kv1.1*$^{V408A/+}$ animals and Ca^{2+} imaging experiments indicates that the spontaneous discharges occur in branches of the nerve, although it does not exclude the involvement of the terminals.

It has been shown that both homomeric *Kv1.1* and heteromeric channels comprised of *Kv1.1* and *Kv1.2* subunits contribute significantly to setting the resting potential of transfected cells and that EA1 mutations impair this function. Moreover, the mutation V408A reduces markedly both the mean-open duration and the deactivation rates of the channel and slightly lowers surface expression (D'Adamo *et al.,* 1999). These effects may increase the excitability of branch points and axons, where *Kv1.1*/*Kv1.2* channels are highly clustered, by shifting their resting potentials to more

depolarized values. As a consequence, discharges may occur spontaneously in axons and action potential propagation failures at branch points may be reduced. During intense neuronal activity the C-type inactivation of Kv channels accumulates modifying both the firing rate and the shape of the action potential (Aldrich *et al.*, 1979). V408A channels enter the C-type inactivated state with a faster rate constant (D'Adamo *et al.*, 1999). Thus, during high frequency spiking, the accumulation of this inactivation process may further reduce the availability of channels, further increasing the juxtaparanodal membrane resistance. As a result, the length constant of the axon would increase and the current is able to spread further along the inner conducting core. These effects may contribute to further exacerbate bursting activity during fatigue in *Kv1.1*$^{V408A/+}$ mice where this mutation has been inserted. Thus, in physiological conditions *Kv1.1* channels may enable sciatic nerve to dampen the node-inter-node electrotonic coupling and prevent re-entrant excitation.

It should also be mentioned that during intense activity K^+ ions accumulate in the tiny peri-internodal space reaching concentrations ranging between 20 to 100 mM. Thus, the above mentioned V408A channel dysfunctions may decrease K^+ accumulation in the peri-internodal space. Low extracellular K^+ concentrations during high frequency spiking may render the nerve re-excitable and result in repetitive discharges.

Super-excitability induced by muscle fatigue, ischemia and temperature

It is know that fatigue intensifies myokymia and body stiffness and precipitates attacks of generalized ataxia in individuals affected by EA1. Here we found that fatiguing stimulations of *LG* nerve-muscle of *Kv1.1*$^{V408A/+}$ mice, in isometric condition, enhance spontaneous and evoked EMG activity. Also an enhancement of the mCAP was observed from *Kv1.1*$^{V408A/+}$ mice that is consistent with increased nerve excitability in response to electrical stimuli. In fact, the electrical stimulation (which was set at 50% of the intensity required to evoke the maximal mCAP amplitude) may be able to recruit other motor units, normally under-threshold, or vary their conduction to increase synchrony. Spontaneous and evoked activities increased a few minutes after fatigue and then

decreased in parallel with fatigue recovery. The causative role of nerve hyper-activation and muscle movement in the excitability enhancement seems to be of minor importance, since it was not observed after the delivery of HFS trains in "quasi isotonic" condition, whereby the nerve was hyper-activated, as in isometric condition but, the muscle presented large displacements in response to each stimulation train and did not exhibit fatigue. Moreover, there was a direct relationship between the mCAP amplitude increase and the degree of fatigue. Therefore, muscle fatigue is crucial for triggering bursting activity and it may depend on a "muscular factor" which modulates pathways also interfering with nerve excitability. The activity-induced K^+ efflux, lactic acid production, pH changes and inorganic phosphate (Pi) accumulation are some of the events mediating muscle fatigue. The concentration of these factors change remarkably in the interstitium during fatigue and by diffusing to nerve structures may contribute to the phenomena observed from *Kv1.1*$^{V408A/+}$ mice. On the other hand, normally functioning *Kv1.1* channels present at the level of the axon of *Kv1.1*$^{+/+}$ animals appear to counterbalance this effect maintaining the excitability of these structures within a physiological range.

As regards the super-excitability induced by ischemia, it is known that in some EA1 individuals myokymic activity becomes apparent from the EMG recording only after the application of regional ischemia (Pessia and Hanna, 2010). We observed, from mutated animals only, that ischemia induced abnormal bursting activity characterized by random singlets, duplets and multiplets and mCAP enhancement. However, there was no difference in the effect of ischemia on muscle tension in either mutated or wild-type animals, as shown indirectly by the twitch amplitude decay, during the ischemic period and its recovery. Noteworthy, Brunt and Van Weerden (1990) reported a recruitment of new and large multiplets, enlargement of pre-existing complexes with extra spikes following ischemia in EA1 individuals. This excess of activity began 0.5-1 min after reversal of ischemia, reached a maximum at 2-5 min and gradually declined over 10-15 min. Strikingly, both the time course and the overall appearance of burst activity in *Kv1.1*$^{V408A/+}$ mice, during ischemia and reperfusion, match that reported for affected individuals, suggesting that similar mechanisms

underlie these responses in rodents and humans. During the initial ischemic insult there is a conversion of muscle metabolism from aerobic to anaerobic that provokes increased concentrations of H^+, ATP depletion, release of K^+ and of Pi. Noticeably, some of these events also induce muscle fatigue. It is then possible that these factors, individually or jointly, may exacerbate the excitability of myelinated nerves and trigger bursting activity in *Kv1.1*$^{V408A/+}$ mice since the mutated channels are unable to counteract their effects.

The action of temperature is less straightforward in EA1 patients. The exposure of the forearm to warm or cold temperatures may increase or decrease myokymic activity recorded from a hand muscle. We consistently observed that temperatures lower than 28°C induce bursting activity in response to nerve stimulation of adult *Kv1.1*$^{V408A/+}$ mice only. In addition, it is likely that the effect of cooling is always to enhance the evoked response, since a low temperature slightly reduced the amplitude of mCAP in *Kv1.1*$^{+/+}$ mice, whereas it slightly enhanced the mCAP in *Kv1.1*$^{V408A/+}$ mice. These findings demonstrate that the V408A mutation in *Kv1.1* channels confers marked temperature-sensitivity to neuromuscular transmission in adult *Kv1.1*$^{V408A/+}$ ataxia mice, similarly to young *Kv1.1* knock-out mice (Zhou et al., 1998). A number of cellular mechanisms may explain the cold induced hyper-excitability, including the temperature-dependence of ion channel kinetics and of the AP shape. Zhou *and colleagues* (1998) proposed the mechano-induced and cholinergic autoreceptor-induced activity as the two likely mechanisms involved in the temperature-sensitivity of *Kv1.1* knock-out mice. Whether or not these apply to *Kv1.1*$^{V408A/+}$ ataxia mice still remains to be investigated.

Abnormal bursting activity does not alter the morphology of LG muscle of Kv1.1$^{V408A/+}$ *mice*

Bilateral calf hypertrophy, enlargement of type I and type II gastrocnemius muscle fibers and variable glycogen depletion have been observed in some EA1 individuals (Van Dyke et al., 1975; Demos et al., 2009; Kinali et al., 2004). Since these changes have not been consistently reported among patients, a noticeable interfamilial and intrafamilial phenotypic variability can be invoked to

account for these observations. The optical and electron microcopy analysis of *LG* muscles from *Kv1.1*$^{V408A/+}$ mice did not reveal obvious changes in fibers types, neuromuscular junction and vascularization. This evidence suggests that anomalous bursting activity may not be sufficiently intense so as to induce muscle transformation and mechanical changes in *Kv1.1*$^{V408A/+}$ mice, during their development through adulthood. Whether the variability in repetitive muscle activation and excitability increment observed in EA1 individuals underlies the inconsistent effect on muscle morphology remains to be explored.

Overall, this study points out that *Kv1.1*$^{V408A/+}$ ataxia mice recapitulate some neuromuscular defects reported for EA1 individuals and represent an excellent animal model for the study of mechanisms precipitating attacks of disabling symptoms. In addition, the insertion of V408A mutation in mammals provides a unique tool for the manipulation of neuromuscular transmission, which cannot be achieved by pharmacological intervention and, helps in the identification of the physiological workings of the PNS.

Conclusion

We show that *Kv1.1* channels with altered function result in hyper-excitability of the sciatic nerve that generates discharges spontaneously, without the influence of the CNS. Stress events such as fatigue, ischemia and lower temperatures further exacerbate motor units excitability. Furthermore, our study sheds new light on the functional role played by axonal *Kv1.1* channels that appear to regulate motor units excitability during the course of muscle fatigue, when the motor nerve could be exposed to physiological factor(s) that interfere with nerve excitability and impulse conduction.

REFERENCES

Adelman JP, Bond CT, Pessia M, Maylie J (1995) Episodic ataxia results from voltage-dependent potassium channels with altered functions. Neuron 15:1449-54.

Aldrich, R.W.Jr, Getting, P.A., and Thompson, S.H. (1979) Mechanism of frequency-dependent broadening of molluscan neurone soma spikes. J Physiol 291**:** 531-544.

Arroyo EJ, Xu YT, Zhou L, Messing A, Peles E, Chiu SY, Scherer SS (1999) Myelinating Schwann cells determine the internodal localization of Kv1.1, Kv1.2, Kvbeta2, and Caspr. J Neurocytol 28: 333-47.

Brunt ERP, van Weerden TW (1990) Familial paroxysmal kinesigenic ataxia and continuous myokymia. Brain 113: 1361–1382.

Chiu SY, Zhou L, Zhang CL, Messing A (1999) Analysis of potassium channel functions in mammalian axons by gene knockouts. J Neurocytol 28: 349-64.

Chiu SY (2011) Matching mitochondria to metabolic needs at nodes of ranvier. Neuroscientist 17: 343-50.

D'Adamo MC, Imbrici P, Sponcichetti F, Pessia M (1999) Mutations in the KCNA1 gene associated with episodic ataxia type-1 syndrome impair heteromeric voltage-gated K(+) channel function. Faseb J 13: 1335-45.

D'Adamo MC, Liu Z, Adelman JP, Maylie J, Pessia M (1998) Episodic ataxia type-1 mutations in the hKv1.1 cytoplasmic pore region alter the gating properties of the channel. Embo J 17: 1200-7.

Demos MK, Macri V, Farrell K, Nelson TN, Chapman K, Accili E, Armstrong L (2009) A novel KCNA1 mutation associated with global delay and persistent cerebellar dysfunction. Mov Disord 24:778-82.

Eunson LH, Rea R, Zuberi SM, Youroukos S, Panayiotopoulos CP, Liguori R, Avoni P, McWilliam RC, Stephenson JB, Hanna MG, Kullmann DM, Spauschus A (2000) Clinical, genetic, and expression studies of mutations in the potassium channel gene KCNA1 reveal new phenotypic variability. Ann Neurol 48:647-56

Herson PS, Virk M, Rustay NR, Bond CT, Crabbe JC, Adelman JP, Maylie J (2003) A mouse model of episodic ataxia type-1. Nat Neurosci 6: 378–383.

Kinali M, Jungbluth H, Eunson LH, Sewry CA, Manzur AY, Mercuri E, Hanna MG, Muntoni F (2004) Expanding the phenotype of potassium channelopathy: severe neuromyotonia and skeletal deformities without prominent episodic ataxia. Neuromuscul Disord 14: 689–693.

Kullmann DM (2010) Neurological channelopathies. Ann Rev Neurosci 33: 151-72.

Lev-Ram V, Ellisman MH (1995) Axonal activation-induced calcium transients in myelinating Schwann cells, sources, and mechanisms. J Neurosci 4: 2628-37.

MacLean JN, Yuste R (2005) A practical guide: imaging action potentials with calcium indicators. In*:* Imaging in neuroscience and development (Yuste R, Konnerth A. ed) pp351-355. New York: Cold Spring Harbor Laboratory Press.

Pessia M, Hanna M (2010) Episodic Ataxia type 1. In GeneReviews [Internet] (Pagon RA, Bird TC, Dolan CR, Stephens K ed). University of Washington, Seattle.

Poliak S, Gollan L, Martinez R, Custer A, Einheber S, Salzer JL, Trimmer JS, Shrager P, Peles E (1999) Caspr2, a new member of the neurexin superfamily, is localized at the juxtaparanodes of myelinated axons and associates with K+ channels. Neuron 24: 1037-47.

Rajakulendran S, Schorge S, Kullmann DM, Hanna MG (2007) Episodic ataxia type 1: a neuronal potassium channelopathy. Neurotherapeutics 2: 258-266.

Ren Y, Ridsdale A, Coderre E, Stys PK (2000) Calcium imaging in live rat optic nerve myelinated axons in vitro using confocal laser microscopy. Journal of Neuroscience Methods 102: 165-176.

Shook SJ, Mamsa H, Jen JC, Baloh RW, Zhou L (2008) Novel mutation in *KCNA1* causes episodic ataxia with paroxysmal dyspnea. Muscle Nerve 37:399-402

Tsaur ML, Sheng M, Lowenstein DH, Jan YN, Jan LY (1992) Differential expression of K+ channel mRNAs in the rat brain and down-regulation in the hippocampus following seizures. Neuron 8: 1055-67.

Vacher H, Mohapatra DP, Trimmer JS (2008) Localization and targeting of voltage-dependent ion channels in mammalian central neurons. Physiol Rev 88: 1407-47.

Van Dyke DH, Griggs RC, Murphy MJ, Goldstein MN (1975) Hereditary myokymia and periodic ataxia. J Neurol Sci 25: 109–118.

Wang H, Kunkel DD, Martin TM, Schwartzkroin PA, Tempel BL (1993) Heteromultimeric K+ channels in terminal and juxtaparanodal regions of neurons. Nature 365: 75–79.

Wang H, Kunkel DD, Schwartzkroin PA, Tempel BL (1994) Localization of Kv1.1 and Kv1.2, two K^+ channel proteins, to synaptic terminals, somata, and dendrites in the mouse brain. J Neurosci 14: 4588-4599.

Zanotti S, Negri T, Cappelletti C, Bernasconi P, Canioni E, Di Blasi C, Pegoraro E, Angelini C, Ciscato P, Prelle A, Mantegazza R, Morandi L, Mora M (2005) Decorin and biglycan expression is differentially altered in several muscular dystrophies. Brain 128: 2546-55.

Zerr P, Adelman JP, Maylie J (1998) Episodic ataxia mutations in Kv1.1 alter potassium channel function by dominant negative effects or haploinsufficiency. J Neurosci 18:2842-8.Zhang CL, Wilson JA, Williams J, Chiu SY. (2006). Action potentials induce uniform calcium influx in mammalian myelinated optic nerves. J Neurophysiol 6: 695-709.

Zhang CL, Ho PL, Kintner DB, Sun D, Chiu SY (2010) Activity-dependent regulation of mitochondrial motility by calcium and Na/K-ATPase at nodes of Ranvier of myelinated nerves. J Neurosci 30: 3555-66.

Zhou L, Messing A, Chiu SY (1999) Determinants of excitability at transition zones in Kv1.1-deficient myelinated nerves. J Neurosci 19: 5768-81.

Zhou L, Zhang CL, Messing A, Chiu SY (1998) Temperature-sensitive neuromuscular transmission in Kv1.1 null mice: role of potassium channels under the myelin sheath in young nerves. J Neurosci 18: 7200-7215.

Zhou L and Chiu SY (2001) Computer model for action potential propagation through branch point in myelinated nerves. J Neurophysiol 85:197-210.

FIGURE LEGENDS

Figure 1

$Kv1.1^{V408A/+}$ ataxia mice display spontaneous muscle discharges

EMG recordings from *LG* muscles of *$Kv1.1^{+/+}$* (*top traces*) and *$Kv1.1^{V408A/+}$* (*bottom traces*) showing the spontaneous activity (***A***) and that following the nerve-evoked mCAP (***B***). Enlargements of the traces are reported below to show the shape of the spontaneous and evoked repetitive muscle activity for *$Kv1.1^{V408A/+}$* that was absent in all *$Kv1.1^{+/+}$* mice tested. (***C***) Bar graphs showing the averaged values of the integrated bursting activity normalized to the integrated mCAP (EMG/mCAP) either in resting conditions (*spontaneous*) or during the post-stimulus periods (*evoked*) for both *$Kv1.1^{+/+}$* (*open bars,* n = 10) and *$Kv1.1^{V408A/+}$* mice (*dashed bars,* n = 10). Note that for *$Kv1.1^{V408A/+}$* mice the evoked EMG activity is remarkable higher also compared to their own spontaneous level of activity (**p<0.01, ***p<0.001). (***D***) Plot of the EMG activity evoked in *$Kv1.1^{V408A/+}$* mice as a function of time. The integrated values were calculated just after the mCAP and multiplied by 10. Note that the single shock stimulation of the motor nerve elicited an immediate induction of EMG activity, followed by a second peak 400-600 msec later that gradually decayed. Data are means ± SEM of 10 animals.

Figure 2

Ca^{2+} signals occur spontaneously within the sciatic nerve of $Kv1.1^{V408A/+}$ ataxia mice

Representative traces showing changes in Ca^{2+} signals over time recorded from the sciatic nerve of $Kv1.1^{+/+}$ (***A***) and $Kv1.1^{V408A/+}$ (***B***) mice. (***C***) Bar graph showing the averaged values of the integrated fluorescence signals ($\Delta F/F_o$) for both $Kv1.1^{+/+}$ (*open bars*, n = 5) and $Kv1.1^{V408A/+}$ mice (*dashed bars*, n = 5). Note that the integrated Ca^{2+} fluorescence recorded in resting conditions from the sciatic nerves of $Kv1.1^{V408A/+}$ mice is remarkable higher then in normal animals (ANOVA;***p<0.001). (***D***) Bar graph showing the number of ΔF data points that lay outside three standard deviations from the mean fluorescence recorded from the sciatic nerves of both $Kv1.1^{+/+}$ (*open bars*) and $Kv1.1^{V408A/+}$ (*dashed bars*; χ^2 analysis: ***p<0.001). (***E***) Representative series of two-photon imaging acquired before (*top panel*) and during the occurrence of abnormal Ca^{2+}signals (*bottom panel*, *boxed area*) in a small branch of the sciatic nerve visualized within a *LG* muscle dissected from a $Kv1.1^{V408A/+}$ mouse.

Figure 3

Fatigue of LG muscle induced by high frequency motor nerve stimulation

Sample traces showing muscle fatigue induced from $Kv1.1^{V408A/+}$ mice by HFS trains in isometric condition (***A***) and "quasi-isotonic condition" (***B***). Twitch (*arrow*) and tetanic (*filled circle*) muscle contractions were elicited before and after fatiguing stimulation. Note the remarkable tension decrease that occurred only in isometric condition. (***C-E***) Bar graphs showing the effect of fatigue, induced in isometric condition, on muscle tension decrease (***C***; the values were calculated at the end of HFS trains), time constants of tetanic tension decay (***D***; peak tension values were fitted with a single exponential function) and fatigue index (***E***; tension $_{(2'\ min)}$/ tension $_{(1'\ min)}$ for $Kv1.1^{+/+}$ (*open bars*) and $Kv1.1^{V408A/+}$ (*dashed bars*) mice. (***F***) Time course of the recovery from muscle fatigue for $Kv1.1^{+/+}$ *(open square)* and $Kv1.1^{V408A/+}$ *(filled square)*. Concerning the overall effects of fatigue,

note that there is no significant difference between the two groups of animals ($p>0.05$). Data are means ± SEM of 15 animals.

Figure 4

Fatiguing HFS trains enhance spontaneous and evoked bursting activity in Kv1.1$^{V408A/+}$ mice

Cartoon showing the experimental configuration for EMG recording and muscle fatigue induction (*inset on the left hand side up*). (***A***,***B***) Sample traces of EMG recorded from *LG* muscles of *Kv1.1*$^{+/+}$ (***A***) and *Kv1.1*$^{V408A/+}$ (***B***) mice showing the spontaneous activity and that evoked by motor nerve stimulation. Recordings were performed before (*pre*) and at different periods elapsing from the delivery of HFS trains (*time reported on the left side*). (***C***,***D***) Plots showing the spontaneous (***C***; n=10) and evoked (***D***; n= 15) integrated EMG activity determined before and after fatiguing stimulation (indicated by a horizontal bar: HFS) for both *Kv1.1*$^{+/+}$ (*open square*) and *Kv1.1*$^{V408A/+}$ (*filled square*) mice. The time course of the recovery of twitch tension from fatigue (*dotted line*) is reported above each plot for direct comparison. Note that only in *Kv1.1*$^{V408A/+}$ mice fatiguing stimulations increase remarkably both the spontaneous and evoked EMG activity. Respectively, these bursting activities reached a peak ~15 and ~10 min after HFS trains. (***E***) Plot of the integrated EMG activity for *Kv1.1*$^{V408A/+}$ mice determined during 1 sec epoch elapsing from the sciatic nerve stimulation. Note that the electric shock induces an immediate increase of the EMG activity, followed by a second peak 300-400 msec later.

Figure 5

Fatiguing HFS trains increase the mCAP of Kv1.1$^{V408A/+}$ mice

mCAP evoked from *LG* muscles of *Kv1.1*$^{+/+}$ (***A***) and *Kv1.1*$^{V408A/+}$ (***B***) mice and recorded before (*pre*) and after the delivery of HFS trains (*the time at which the evoked potentials are recorded and analyzed is reported on the left hand side*). (***C***) Plot of the integrated mCAP as a function of time elapsing from HFS trains delivery and normalized to pre-fatigue value for *Kv1.1*$^{V408A/+}$ (*filled*

square; n= 15) and *Kv1.1*$^{+/+}$ (open square; n= 15) mice. The time course of the recovery of twitch tension from fatigue (*dotted line*) is reported above the plot for direct comparison. Note that fatiguing stimulations increase remarkably the mCAP of *Kv1.1*$^{V408A/+}$ mice, which reached a peak 15 min after the delivery of HFS trains. Conversely, the same procedure reduced slightly the mCAP of *Kv1.1*$^{+/+}$ muscles.

Figure 6

Dependence of EMG responses to nerve stimulation intensity

(***A***) Bar graph of the evoked EMG bursting activity elicited by HFS trains and integrated in either isometric or "quasi-isotonic" condition (n= 5). Note that the bursting activity in isometric condition was significantly higher than quasi-isotonic condition (***p<0.001). (***B***) Integrated mCAP values were determined in either "quasi isotonic" condition, upon the delivery of HFS trains lasting 180 sec (*isotonic*) or in isometric condition by varying the duration of HFS trains from 30 to 180 sec. This procedure was used to induce different degrees of fatigue. The circles include the responses of four *Kv1.1*$^{V408A/+}$ mice under the conditions indicated on the right hand side. Linear regression was used to fit the data points (*dashed line*). Note that the integrated mCAP values increase linearly with the intensity of the stimulations.

Figure 7

Normal morphology of LG nerve-muscle of Kv1.1$^{V408A/+}$ *mice.*

(***A***) Representative photomicrographs of *LG* muscles and of neuromuscular junctions from *Kv1.1*$^{V408A/+}$ (*top panels*) and *Kv1.1*$^{+/+}$ (*bottom panels*) mice. The morphology of the muscle was analyzed by Gomori Trichrome (GTR) and Hematoxylin-Eosin (H&E) and the fiber type composition by NADH (x200). (***ElM***) Electron microscopy photomicrographs of the neuromuscular junctions (x4400). Frequency distribution for type I (***B, C***) and type II (***E, F***) muscle fibers calculated for the mouse strains indicated on top. Bar graphs showing the average diameter of fiber

type I (***D***) and type II (***G***) for *Kv1.1*$^{+/+}$ and *Kv1.1*$^{V408A/+}$ muscles. Note that muscle morphology and fiber type composition were normal for both *Kv1.1*$^{+/+}$ and *Kv1.1*$^{V408A/+}$ mouse strains.

Figure 8

The distribution and dimension of capillaries in LG muscle is similar between Kv1.1$^{+/+}$ *and Kv1.1*$^{V408A/+}$ *mice*

(***A***) Immunostaining of capillaries with GSL I for the indicated mouse strains (x400). Bar graphs showing the mean diameter of capillaries (***B***) and the number of capillaries per mm^2 (***C***) in the *LG* muscle dissected from the two groups of animals.

Figure 9

Effects of ischemia on the mechanical responses and EMG activity of LG muscle

Cartoon showing the experimental configuration (*inset on the left hand side up*). (***A***) Muscle twitch tension decrease during and after 3 min of occlusion of artery and venous blood vessels supplying the *LG* muscle of *Kv1.1*$^{+/+}$ (*open squares*) and *Kv1.1*$^{V408A/+}$ (*filled squares*) mice. The horizontal bars marked I (*ischemia*) in panels ***A***, ***D***, ***E*** indicate the period during which ischemia was induced. (***B,C***) EMG recordings from *LG* muscles of *Kv1.1*$^{+/+}$ (***B***) and *Kv1.1*$^{V408A/+}$ mice (***C***) after sciatic nerve stimulation by single electric shock. The representative traces were recorded before (*pre*), during ischemia and at different periods following the reperfusion of the *LG* nerve and muscle (*indicated on the left hand side of traces*). Note that while this procedure does not affect the EMG responses from *Kv1.1*$^{+/+}$, it exacerbates delayed bursting activity in *Kv1.1*$^{V408A/+}$ animals. (***D***) Time course of integrated and normalised EMG bursting activity for *Kv1.1*$^{+/+}$ (*open squares*; n =5) and *Kv1.1*$^{V408A/+}$ (*filled squares*; n =5) before, during and after ischemia. The twitch tension decrease (*dotted line*) is timely matched above plots ***D*** and ***E*** for direct comparison. (***E***) Plot of the integrated mCAP before, during and after ischemia for both *Kv1.1*$^{+/+}$ (*open squares*) and *Kv1.1*$^{V408A/+}$ (*filled squares*) mice. Note that both bursting activity and the mCAP were increased remarkably by

ischemia in *Kv1.1*$^{V408A/+}$ mice. These effects were maximal just after blood re-perfusion, while the twitch tension reduction was maximal at the third minute of ischemia (*dotted line*). Conversely, ischemia reduced slightly and temporarily the mCAP in *Kv1.1*$^{+/+}$ mice (n=5; *p<0.05). (***F***) Plot of the integrated EMG activity for *Kv1.1*$^{V408A/+}$ mice determined during 1 sec epoch elapsing from the sciatic nerve stimulation. Note that the electric shock induces an immediate increase of the EMG activity followed by a second peak ~400 msec later and a gradual decay to pre-stimulus values.

Figure 10

Effects of temperature on EMG activity of LG muscle

Cartoon showing the experimental configuration (*inset on the left hand side up*). EMG recordings from *LG* muscles of *Kv1.1*$^{+/+}$ (***A***) and *Kv1.1*$^{V408A/+}$ (***B***) upon sciatic nerve stimulation. The representative traces were recorded while varying the temperature of the *LG* muscle-nerve preparation gradually from 36°C to 22°C and back to 36°C (*reported on the left hand side of sample traces).* Note that cooling exacerbates delayed bursting activity in *Kv1.1*$^{V408A/+}$ while it does not affect the responses of *Kv1.1*$^{+/+}$ animals. (***C***) Averaged EMG activity estimated as integral of the entire post-stimulus periods and every two degrees of cooling for *Kv1.1*$^{+/+}$ (*open squares*; n = 7) and *Kv1.1*$^{V408A/+}$ (*filled squares*; n = 7). Note that bursting activity was exacerbated by cooling below ~28°C and reached maximal intensity at 22°C. (***D***) Averaged EMG activity recorded at 22°C, expressed as integrated values and plotted as a function of the post-stimulus duration for both *Kv1.1*$^{+/+}$ (*open square*) and *Kv1.1*$^{V408A/+}$ (*filled square*) mice. Note that bursting activity reached the maximal intensity ~100 msec after the electric shock and declined thereafter. (***E***) Bar graph of the integrated mCAP recorded at 22° from *Kv1.1*$^{+/+}$ (*open bar*) and *Kv1.1*$^{V408A/+}$ (*dashed bar*) mice normalized to the mCAP recorded at 36°C (n=7; *p<0.05).

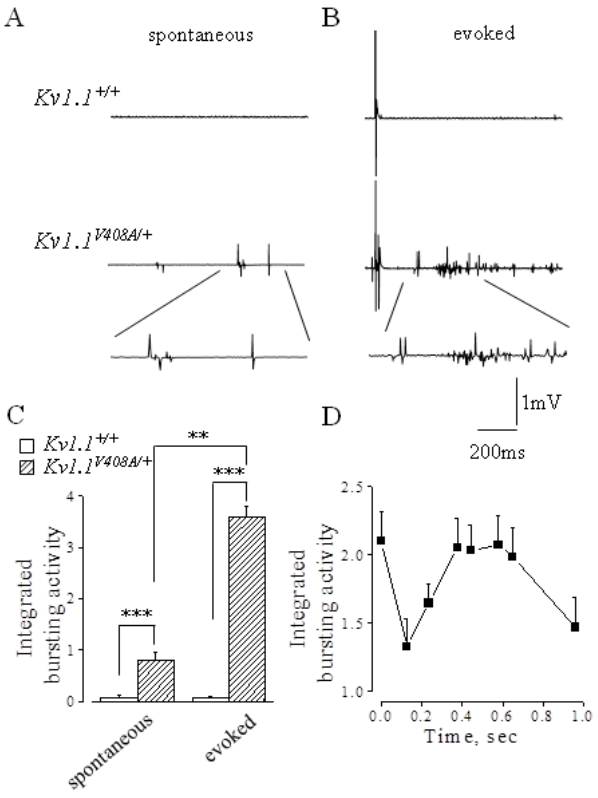
A
spontaneous
B
evoked
Kv1.1+/+
Kv1.1V408A/+
1mV
200ms
C
Kv1.1+/+
Kv1.1V408A/+
**
***
***
Integrated bursting activity
0
1
2
3
4
spontaneous
evoked
D
Integrated bursting activity
1.0
1.5
2.0
2.5
0.0
0.2
0.4
0.6
0.8
1.0
Time, sec

Figure 1

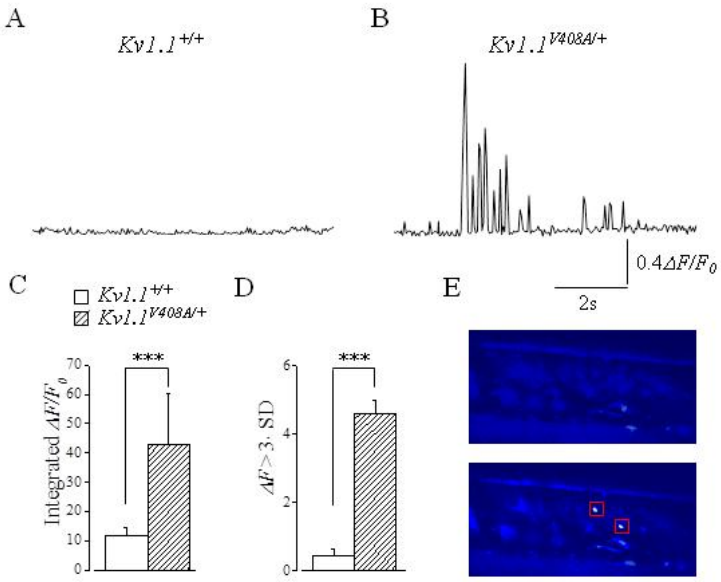
A
Kv1.1+/+
B
Kv1.1V408A/+
0.4ΔF/F0
2s
C
Kv1.1+/+
Kv1.1V408A/+
***
Integrated ΔF/F0
D
***
ΔF>3. SD
E

Figure 2

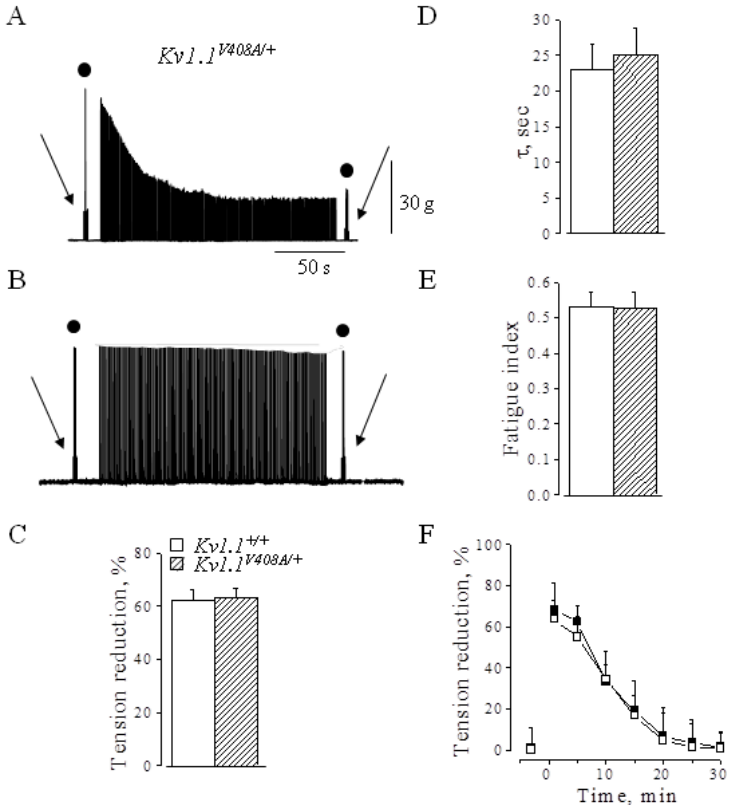
A
Kv1.1V408A/+
30 g
50 s
B
C
Kv1.1+/+
Kv1.1V408A/+
Tension reduction, %
D
τ, sec
E
Fatigue index
F
Tension reduction, %
Time, min

Figure 3

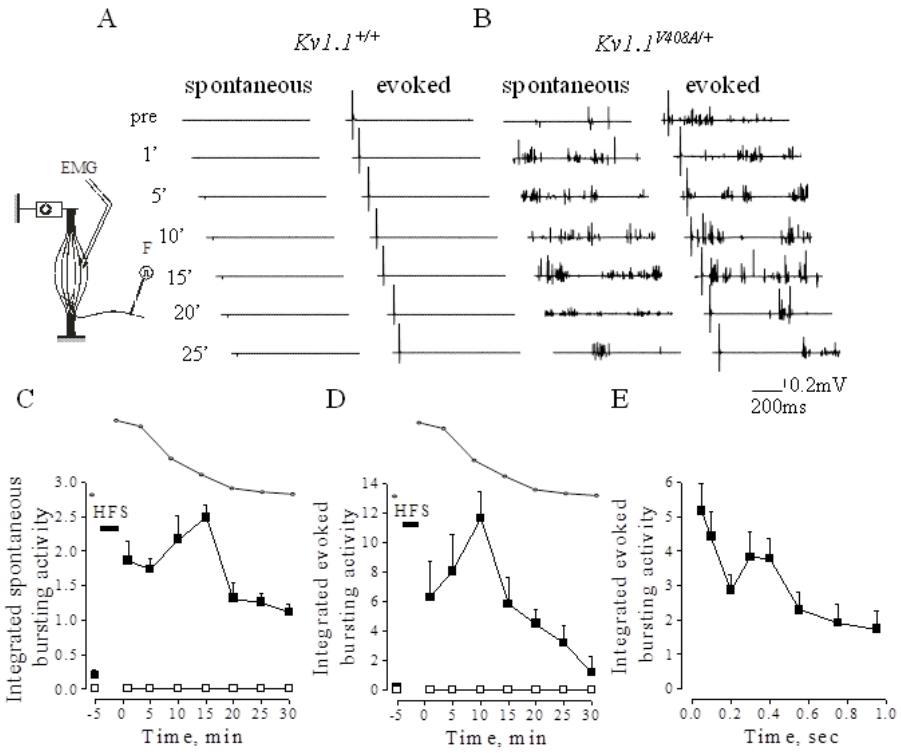
A
B
Kv1.1+/+
Kv1.1V408A/+
spontaneous
evoked
spontaneous
evoked
pre
1'
5'
10'
15'
20'
25'
EMG
F
0.2mV
200ms
C
D
E
HFS
HFS
Integrated spontaneous bursting activity
Integrated evoked bursting activity
Integrated evoked bursting activity
Time, min
Time, min
Time, sec

Figure 4

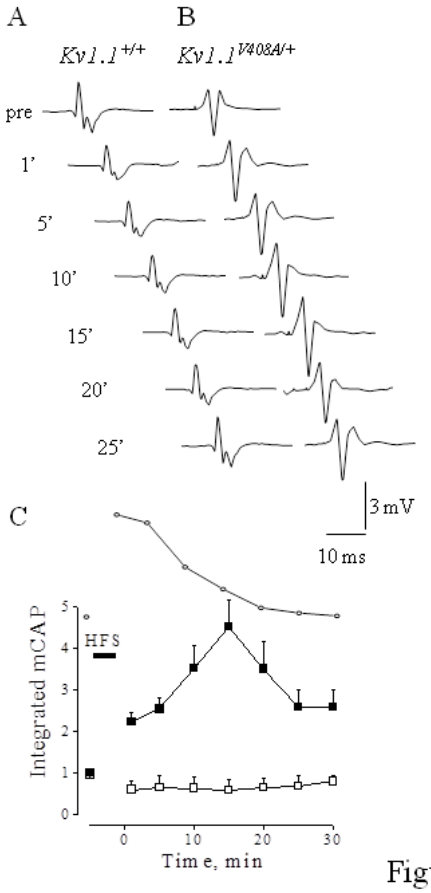
A
B
Kv1.1+/+
Kv1.1V408A/+
pre
1'
5'
10'
15'
20'
25'
3 mV
10 ms
C
HFS
Integrated mCAP
0
1
2
3
4
5
0
10
20
30
Time, min

Figure 5

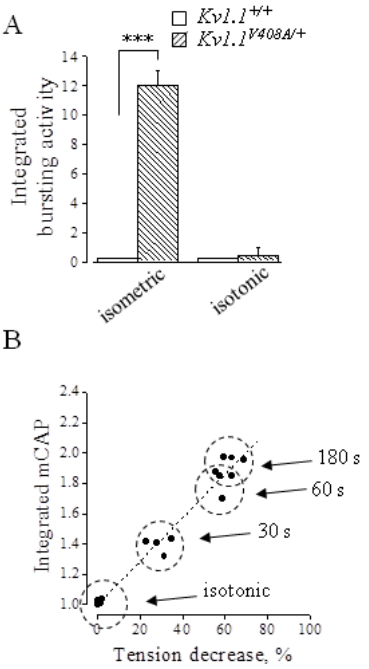
A
Kv1.1+/+
Kv1.1V408A/+
***
Integrated bursting activity
0
2
4
6
8
10
12
14
isometric
isotonic
B
Integrated mCAP
1.0
1.2
1.4
1.6
1.8
2.0
2.2
2.4
180 s
60 s
30 s
isotonic
0
20
40
60
80
100
Tension decrease, %

Figure 6

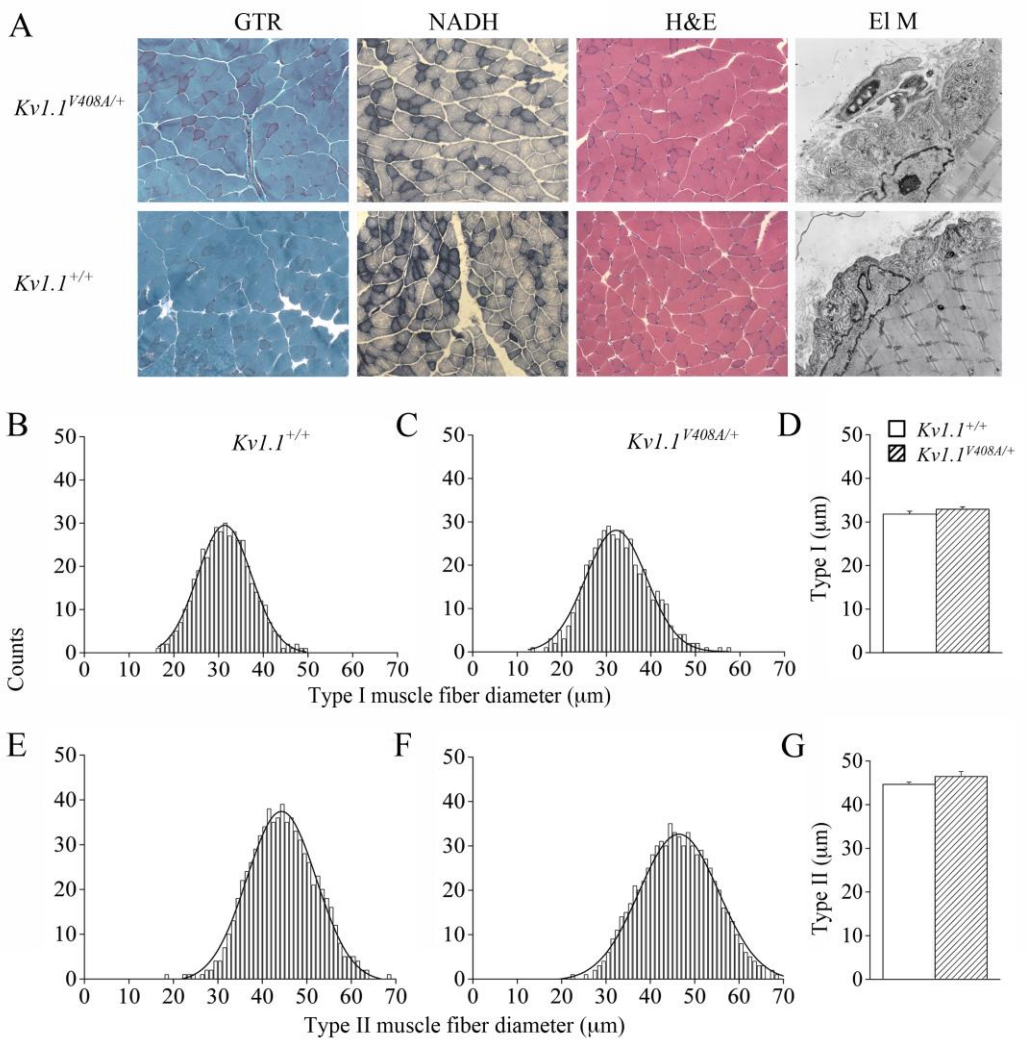
A
GTR
NADH
H&E
El M
Kv1.1V408A/+
Kv1.1+/+
B
Kv1.1+/+
C
Kv1.1V408A/+
D
Kv1.1+/+
Kv1.1V408A/+
Counts
Type I muscle fiber diameter (μm)
Type I (μm)
E
F
G
Type II muscle fiber diameter (μm)
Type II (μm)

Figure 7

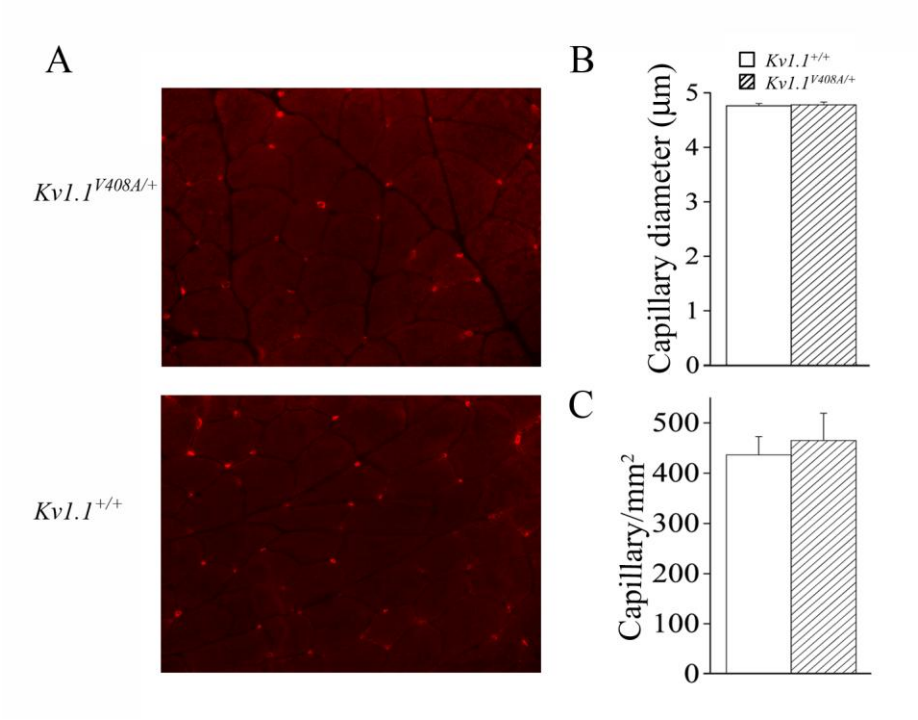

Figure 8

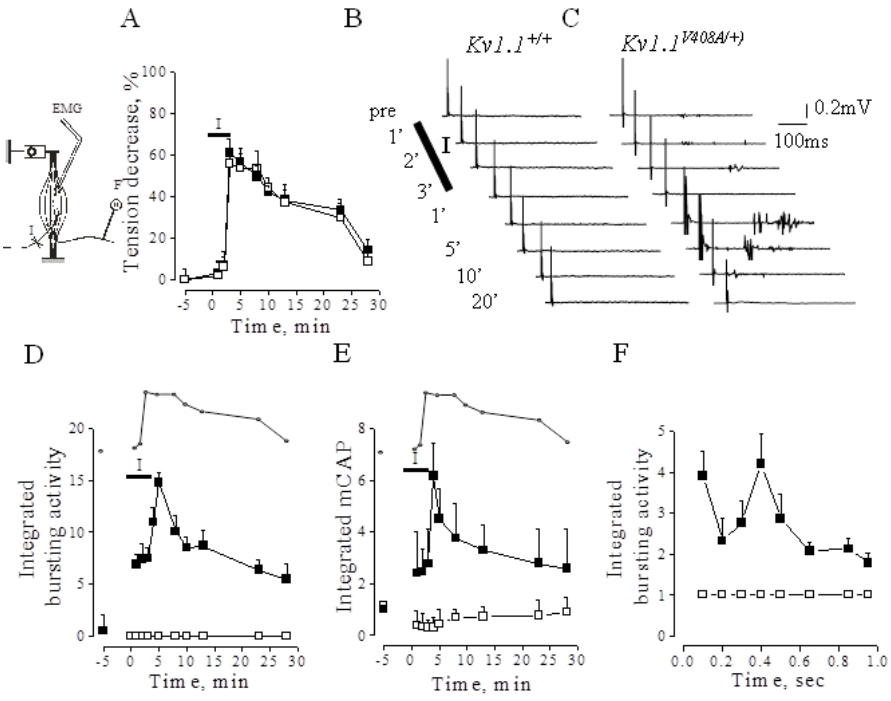

Figure 9

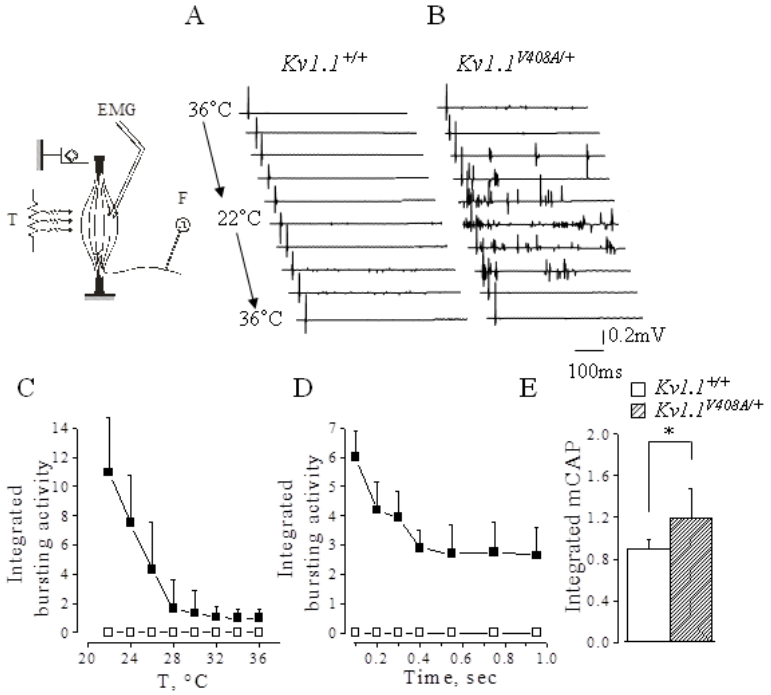

Figure 10

View publication stats